

# PCCP

Accepted Manuscript



This is an *Accepted Manuscript*, which has been through the Royal Society of Chemistry peer review process and has been accepted for publication.

*Accepted Manuscripts* are published online shortly after acceptance, before technical editing, formatting and proof reading. Using this free service, authors can make their results available to the community, in citable form, before we publish the edited article. We will replace this *Accepted Manuscript* with the edited and formatted *Advance Article* as soon as it is available.

You can find more information about *Accepted Manuscripts* in the [Information for Authors](#).

Please note that technical editing may introduce minor changes to the text and/or graphics, which may alter content. The journal's standard [Terms & Conditions](#) and the [Ethical guidelines](#) still apply. In no event shall the Royal Society of Chemistry be held responsible for any errors or omissions in this *Accepted Manuscript* or any consequences arising from the use of any information it contains.

**Keywords:** Density Functional Theory, HSE06, adsorption, TiO<sub>2</sub>, tetra-aza macrocycle, pyridine rings, Porphyrin.

## Non-innocent Adsorption of Co-Porphyrin on Rutile(110)

Yeliz Gurdal,<sup>1,\*</sup> Sandra Luber,<sup>1,†</sup> Jürg Hutter,<sup>1,‡</sup> and Marcella Iannuzzi<sup>1,§</sup>

<sup>1</sup>*Institut für Chemie, Universität Zürich,  
Winterthurerstrasse 190, CH-8057 Zürich, Switzerland*

(Dated: July 29, 2015)

### Abstract

Solar-light driven water splitting is a promising way for sustainable production of molecular hydrogen, the latter representing an efficient carrier for energy storage and conversion into common liquid fuels. In search of novel catalysts for high-performance water splitting devices, Co-porphyrin (CoPy) has been recently synthesized and successfully used as homogeneous water reduction catalyst. We investigate the adsorption of this molecule on rutile TiO<sub>2</sub> (110) surface as a possible first step towards the design of a heterogeneous water reduction system. We find that the adsorption of the molecule is stabilized by the interaction of the cyano groups with the under-coordinated Ti centers present at the surface. This interaction induces the rehybridization of the molecular orbitals localized on the cyano groups and the realignment of the lowest unoccupied molecular states. Moreover, the highest occupied molecular orbital of CoPy@rutile(110) is localized on CoPy and the energy gap turns out to be significantly smaller than the gap of pristine rutile(110). This implies that direct or indirect injections of electrons from CoPy to the rutile (110) surface is in principle possible upon the absorption of light in the visible range. On the other hand, the electronic properties of the Co(II) center are not modified by the adsorption, which suggests that CoPy and its derivatives may be used in water electrolysis for hydrogen production also in the adsorbed state.

## I. INTRODUCTION

In the quest for renewable energy sources molecular hydrogen is one of the most favoured candidate as energy carrier. Compared to other means, such as electricity, bio-fuels, or conventional fuels, hydrogen has the highest specific energy content<sup>1</sup>, and is also environmentally preferable, because the waste product of its reaction with pure oxygen is simply water<sup>2</sup>. However, the large scale production and storage of molecular hydrogen is still an open issue. Several techniques can be employed for its production, such as water electrolysis<sup>3</sup>, steam and ethanol reforming<sup>4,5</sup>, partial oxidation of hydrocarbons<sup>6</sup>, dark fermentation<sup>7</sup>, and photo-chemical water reduction. The latter is of particular interest, because it emulates natural processes and needs only solar light as energy source<sup>8</sup>.

Water reduction in homogeneous environment has been widely studied<sup>9</sup>. Most of the working systems are based on the use of expensive metals as catalytic reduction centers<sup>10</sup>. However, it has been shown that also less expensive Co-based catalysts can be employed for H<sub>2</sub> production with low over-potentials<sup>11</sup>. Peters et al.<sup>12</sup> investigated catalytic activity of several cobalt complexes with BF<sub>2</sub> glyoxime or propane bridged tetraimine ligands in acetonitrile. They concluded that with less electron donating ligands reduction of Co-complexes can be achieved easily, leading to H<sub>2</sub> production. Guttentag et al.<sup>13</sup> studied the activity of [Co<sup>III</sup>Br<sub>2</sub>(DO)(DOH)pn] with photo-sensitizer [Re(CO)<sub>3</sub>(bipy)(py)]<sup>+</sup> in pure water and acidic environment, demonstrating that H<sub>2</sub> production is possible without organic solvents. Macro-cyclic molecules like metal centered porphyrins are also widely studied alternative catalysts, thanks to their low cost and wide range of light absorption capability<sup>14,15</sup>. Solis et al.<sup>16</sup> modeled cobalt hangerman porphyrins in acetonitrile solution and determined the pathway for proton coupled electron transfer for H<sub>2</sub> generation. For recent reviews and studies on homogeneous water reduction we refer to Refs.<sup>17-20</sup>.

In spite of the established achievements in H<sub>2</sub> generation in homogeneous environments, the most important drawback is the rapid recombination of photo-generated products in solution<sup>21</sup>. Therefore, it has been proposed that in heterogeneous environments, where the catalyst is combined with a supporting material, the fast back electron transfer can be prevented and the system is stabilized<sup>22</sup>. Several studies are already available on the properties of metal centered porphyrins adsorbed on TiO<sub>2</sub> surfaces<sup>23-25</sup>.

Only relatively few studies on the combination of Co-complexes with heterogeneous sys-

tems have been published. The Co-based complex  $[\text{Co}^{\text{III}}(\text{dmgH})_2(\text{pyridyl-4-hydrophosphonate})\text{Cl}]$  adsorbed on a  $\text{TiO}_2$  surface via anchoring groups has been considered as catalyst for proton reduction<sup>26</sup>. Yin et al.<sup>27</sup> studied the organic dye eosin Y (EY) and several other Co complexes also adsorbed on the  $\text{TiO}_2$  surface through different anchoring groups. They concluded that  $\text{TiO}_2$  is able to harvest electrons from the excited EY molecules, thus generating long-lived charge-separated states, which eventually lead to the electron transfer to the Co-catalyst and the reduction process. A similar reductive pathway has also been observed by Lakadamyali et al.<sup>28</sup>, who studied the co-adsorption of the CoP catalyst and a ruthenium dye RuP on  $\text{TiO}_2$ . The photo-excitation of RuP induces an electron injection into the conduction band of  $\text{TiO}_2$ . The photo-electrons are then transferred to CoP, where the  $\text{H}_2$  formation occurs. The photo-excitation of Co(I)-porphyrin on  $\text{TiO}_2$  in acetonitrile-pyridine solution has also been studied<sup>29</sup>, showing that after the rapid electron injection from Co to  $\text{TiO}_2$  and the coordination of pyridine to Co, the undesired charge recombination is significantly slowed down.

Among the heterocyclic molecules, the porphyrin derived tetra-aza macro-cycle, constituted of four pyridine rings, is named pyrphyrin (Py) but also known as Ogawa porphyrin like ligand. Pyrphyrin has been introduced first by Ogawa et al.<sup>30</sup> in 1984. Later, alkylated pyrphyrin has also been synthesized and its optical properties have been characterized<sup>31</sup>. More recently, metal-centered pyrphyrins have been studied both experimentally and theoretically to determine their UV-visible spectra in solution<sup>32-34</sup>.

The need for new, promising, and feasible photo-catalysts for water reduction and the unexplored potential of pyrphyrin adsorbed on  $\text{TiO}_2$  surface are the motivations for the present work. To the best of our knowledge, this is the first time that pyrphyrin on semiconductors is investigated. It is generally accepted that anatase phase of  $\text{TiO}_2$  exhibits higher photocatalytic activity than rutile  $\text{TiO}_2$ <sup>35</sup>, which resulted theoretical investigation of water- $\text{TiO}_2$  interactions mostly with the anatase phase<sup>36</sup>. However, in this study only the rutile phase is considered, which is easier to obtain as high quality single crystal<sup>37</sup> and, for this reason, it is going to be employed in upcoming experimental studies of the catalytic activity of supported-CoPy.

We study the structural and electronic properties of the complex, CoPy adsorbed on rutile (110) surface, by means of density functional theory (DFT). In the following, we first briefly describe the applied methodology and the used models for the molecule, the surface and the

complex. Next, we discuss the possible adsorption configurations of CoPy@rutile(110), and finally we analyze in detail the electronic structure of the most stable configuration.

## II. COMPUTATIONAL METHODOLOGY

Electronic structure calculations are performed at the Kohn-Sham DFT level, employing the Gaussian and plane wave (GPW) formalism as implemented in the CP2K/QUICKSTEP package<sup>38</sup>. Double-zeta valence plus polarization (DZVP) basis sets, optimized on molecular geometries (Mol-Opt method)<sup>39</sup>, are employed for all atomic kinds. A cutoff of 600 Ry is used for the auxiliary plane wave basis set. The interaction between the valence electrons and the atomic cores is described through norm-conserving Goedecker–Teter–Hutter (GTH) pseudo potentials<sup>40</sup>. The valence shells contain 12, 6, 17, 4, 1, and 5 electrons for Ti, O, Co, C, H, and N, respectively. Periodic boundary conditions are always applied.

As exchange–correlation functional, the general gradient approximation (GGA) by Perdew–Burke–Ernzerhof (PBE)<sup>41</sup> is used. The dispersion interactions are corrected according to the Grimme–D3 scheme<sup>42</sup> for the optimization of the geometries. This level of theory has been proved to be sufficiently accurate to describe the structural properties of the materials involved in this study. Namely, the lattice parameters of bulk rutile turn out to be in agreement with the experimental values within an error of 1%<sup>43</sup>. However, PBE is known to underestimate the energy gap of TiO<sub>2</sub> as for other oxides<sup>44,45</sup>. The most commonly adopted solution to this deficiency is the use of suitable hybrid functionals that can reproduce the experimental value<sup>46,47</sup>. For the specific case of TiO<sub>2</sub>, we find, in agreement with previous works, that the best accuracy in the energy gap is achieved by applying the Heyd–Scuseria–Ernzerhof (HSE06) hybrid functional<sup>43,48,49</sup>. All hybrid functional calculations are performed with the help of the auxiliary density matrix method (ADMM)<sup>50–52</sup>, which provides a significant speed up and makes it possible to compute the electronic structure of several hundreds of atoms of condensed matter systems. The required ADMM basis sets have been optimized to reproduce the results of full hybrid functional calculations with very high accuracy. Despite the speed up obtained with ADMM, hybrid functional geometry optimization are still computationally very demanding and do not produce important changes with respect to the PBE optimization. Therefore, our strategy consists in carrying out the refinement of the electronic structure of PBE-optimized geometry using the HSE06

hybrid functional.

### III. STRUCTURAL MODELS

#### A. Rutile: Bulk and (110) Surface

The rutile lattice belongs to the  $P4_2/mnm$  (No. 136) tetragonal space group<sup>53,54</sup>. In the bulk, each Ti atom is coordinated by six O atoms, while the O atoms are three-fold coordinated by Ti. In order to assess our PBE computational set up, the lattice parameters are optimized for a  $3\times 3\times 3$  supercell (162 atoms). This supercell is sufficiently large to converge the bulk structural properties, which turn out to be in very good agreement with previously published data, from both experimental and DFT studies (see Table I). The corresponding band gap energies,  $E_{\text{gap}}$ , computed for the PBE and the HSE06 functionals are reported in Table II and also compared to previous studies. All GGA and LDA result underestimate the  $E_{\text{gap}}$  by more than 1.2 eV, while PBE0 overestimates it by about the same amount. Only the value obtained with HSE06 approximates the experiment with reasonable accuracy. The slight discrepancies between results obtained with the same functional can be ascribed to different basis sets and pseudopotentials.

TABLE I: Lattice parameters (a and c) and bulk modulus (B) of bulk  $\text{TiO}_2$ . The values reported for this work are obtained for the  $3\times 3\times 3$  supercell and the PBE functional.

Method	a [ $\text{\AA}$ ]	c [ $\text{\AA}$ ]	B [GPa]	ref.
GGA/PBE/GPW	4.606	2.966	219	this work
GGA/PW92/PAW	4.649	2.972	225	55
GGA/PBEsol/PW	4.604	2.947	-	56
LDA/PAW	4.554	2.927	256	57
Experiment	4.587	2.954	210	58
Experiment	4.594	2.959	-	53

Figure 1 shows projected density of states (PDOS) for O and Ti atoms in bulk rutile. The highest occupied states have O-2p character, whereas the lowest unoccupied states are Ti-3d, in agreement with previously published calculations<sup>60,61</sup>. The hybridization between

TABLE II: Band gap energy ( $E_{\text{gap}}$ ) of bulk  $\text{TiO}_2$ . The values reported for this work are obtained for the  $3 \times 3 \times 3$  supercell.

Method	$E_{\text{gap}}$ [eV]	ref.
GGA/PBE	1.73	this work
GGA/PBE	1.74	59
GGA/PW92	1.80	57
LDA	1.81	57
HSE06	3.35	this work
HSE06	3.11	43
PBE0	4.21	43
Experiment	3.0	58

O-2p and Ti-3d states results in covalent bonding<sup>62</sup>.

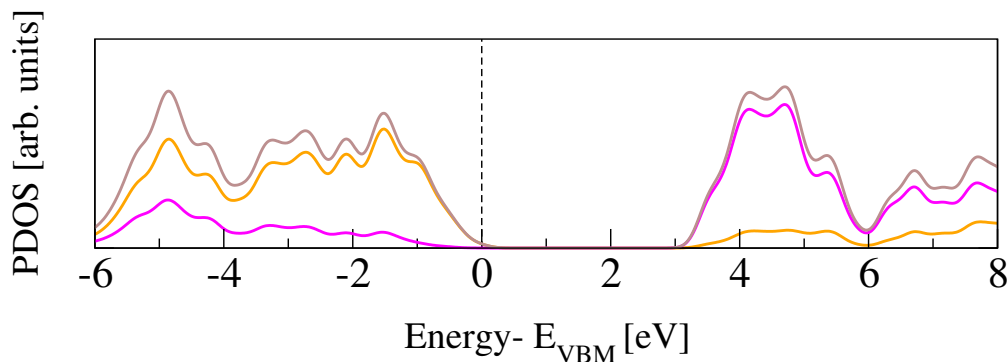


FIG. 1: Density of states of bulk rutile: total DOS plotted with brown line, O PDOS in orange, Ti PDOS in magenta. The distributions are normalized by the number of atoms and the aligned at zero with the valence band maximum (VBM) energy.

The (110) surface is the most stable surface of rutile, and also the most frequently studied and used one for applications<sup>63</sup>. To model such a surface, a symmetric slab consisting of a few atomic layers is cut out from the bulk cleaving along the (110) plane. Above the surface, a sufficiently large amount of vacuum space (20 Å) is added to avoid interactions with the periodic images in the perpendicular direction. The surface unit cell contains two Ti atoms, which lay on the same plane, and four O atoms, two on the same plane as Ti, one above

(sticking out O) and one below. One surface Ti atom is still six-fold coordinated, as in the bulk, while the second is five-fold coordinated. Among the O atoms, three are still three-fold coordinated, while the sticking out one is two-fold coordinated. This latter dangling O atom is a particularly active species, which can lead to the formation of vacancies at the surface, or be saturated. Figure 2 displays the top and side view of a  $3 \times 7$  slab, containing five atomic layers. We label the surface three-fold and two-fold coordinated O atoms with  $O_{3c}$  and  $O_{2c}$ , while the bulk oxygens are labeled  $O_{3c-bulk}$ . We also distinguish between the bulk Ti atoms, labeled  $Ti_{6c-bulk}$ , and the under-coordinated Ti atoms at the surface,  $Ti_{5c}$ . In order to determine the optimal number of layers for the slab model, we tested the convergence of the surface energy. The surface energy is calculated as

$$E_{\text{surface}} = \frac{E_{\text{slab}} - N \cdot E_{\text{bulk}}}{2 \cdot A} \quad (1)$$

where  $E_{\text{slab}}$  is the total energy of the optimized slab model,  $E_{\text{bulk}}$  is the energy per  $TiO_2$  unit in the bulk,  $N$  is the number of units contained in the slab, and  $A$  is the area of the exposed surface.

Slabs from 3 to 9 layers have been considered (see ESI). We conclude that a 5 layer slab is sufficient to model the rutile (110) surface. The surface energy of the  $3 \times 3 \times 5$  slab is  $0.72 \text{ J/m}^2$ , in quite good agreement with the values found in the literature<sup>63</sup>.

The band gap calculated by HSE06 for the rutile slab of five layers, where both exposed surfaces are fully relaxed is  $3.18 \text{ eV}$ , in agreement with the experiment<sup>64</sup>. The reduction of the energy gap at the surface is due to the presence of energy states in the gap, which are generated by electrostatic shifting of  $Ti_{5c}$  states towards  $O_{2c}$  and  $O_{3c-bulk}$  band, also discussed in Ref.<sup>65</sup>. We also computed the electronic properties for slabs of different size, concluding that the slab of five layers is a good compromise between accuracy and efficiency, see ESI.

## B. Pyrphyrin

Ball and stick sketches of Py and CoPy are shown in Figure 3. Py is characterized by CN groups binding to the pyridine rings via  $sp^2$  hybridized bridging carbons. We label the nitrogen atoms of the cyano groups  $N_{CN}$  to distinguish them from the pyridine nitrogens at the center of the molecule ( $N_p$ ). Two  $N_p$  are protonated in Py at anti positions<sup>66</sup>, while the

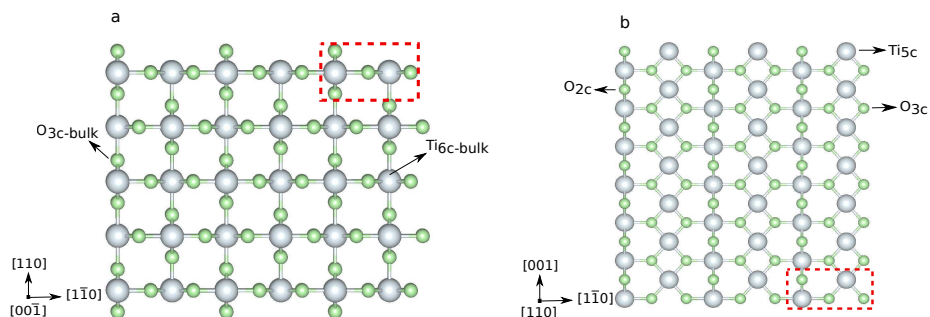


FIG. 2: Ball and stick representation of the rutile (110)  $3 \times 7 \times 5$  slab, where 5 is the number of layers: a) side view and b) top view. For clarity, only topmost atomic layer is shown in (b). Surface atoms are labeled as  $O_{2c}$ ,  $O_{3c}$ , and  $Ti_{5c}$ , bulk atoms as  $O_{3c-bulk}$  and  $Ti_{6c-bulk}$ . The dashed red box indicates the surface unit cell. Color code: light gray: Ti, light green: O.

protons are replaced by the Co(II) cation in CoPy. In the gas phase, both molecules are planar with a vanishing dipole, as discussed in Ref.<sup>34</sup>. In the center of the molecule, the four

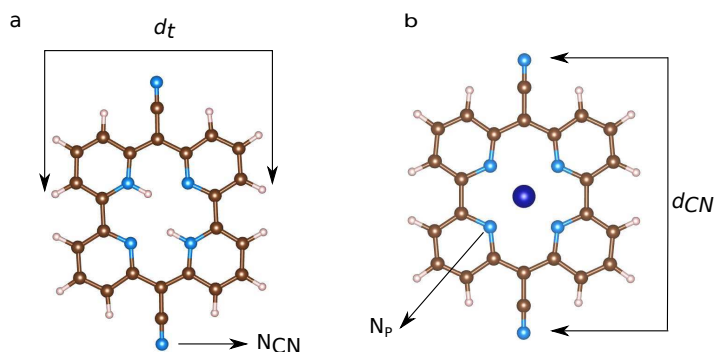


FIG. 3: Ball and stick representations of a) Py and b) CoPy. The molecular size is described by means of the two diameters,  $d_{CN}$  and  $d_t$ . Nitrogens in cyano groups and pyridine rings are labeled as  $N_{CN}$  and  $N_p$ , respectively. Color code: brown: C, light pink: H, dark blue: Co, blue: N.

$N_p$  are symmetrically coordinating Co in CoPy, while the protonated nitrogens in Py are displaced outwards. Along the axis of the cyano groups,  $d_{CN}$ , the molecule is slightly shorter for CoPy with respect to Py, due to the interaction between Co(II) and the electronegative nitrogens. Some structural parameters are reported in Table III.

Table IV shows the energy gaps between the highest occupied molecular orbital (homo) and the lowest unoccupied molecular orbital (lumo) as computed for Py and CoPy with the PBE and HSE06 functionals. The presence of Co(II) slightly reduces the energy gap; the effect is more pronounced with HSE06, for more discussion see ESI. Calculations with CoPy

TABLE III: Selected distances calculated for the optimized geometries of Py and CoPy in the gas phase.

Molecule	Distances	Length [ $\text{\AA}$ ]
Py	$d_{\text{CN}}$	11.96
	$\text{N}_p\text{-N}_p$ (prot.)	3.98
	$\text{N}_p\text{-N}_p$ (not prot.)	3.80
	$d_t$	9.45
CoPy	$d_{\text{CN}}$	11.78
	$\text{N}_p\text{-N}_p$	3.77
	$d_t$	9.57

TABLE IV: Homo-lumo gap ( $E_{\text{gap}}$ ) of Py and CoPy calculated with different density functionals.

Molecule	Functional	$E_{\text{gap}}$ [eV]
Py	PBE	1.52
Py	HSE06	2.23
CoPy	PBE	1.46
CoPy	HSE06	2.03

are always performed with spin polarization. The lowest energy spin state turns out to be a doublet and the spin density is localized exclusively at the Co center. The homo of CoPy in the gas phase has major contributions from the cyano groups, the pyridine carbons, and the  $\text{N}_p$ , but it is also present at Co(II) centers. The lumo, instead, is uniformly distributed over the pyridine CH groups, the central C atoms, and the  $\text{N}_p$ , but it does not have significant contributions from the cyano groups and the Co(II). The two frontier orbitals of the gas phase molecule are displayed in Figure 4.

### C. CoPy Adsorption on Rutile(110)

In order to find possible adsorption sites of CoPy on rutile, it is necessary to explore the potential energy surface of the CoPy@rutile complex. We started eleven independent optimizations, changing the initial coordinates of the gas-phase optimized CoPy on rutile.

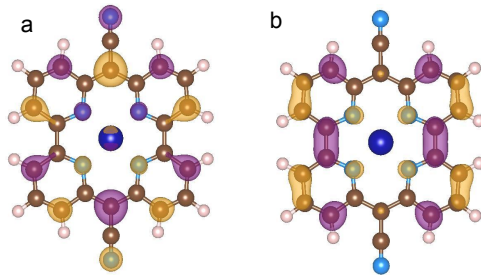


FIG. 4: Homo (a) and lumo (b) of CoPy in the gas phase. The displayed isosurfaces are obtained at the value of  $\pm 0.236 \text{ e}/\text{\AA}^3$ .

The molecule has always been positioned parallel to the surface at a distance a few  $\text{\AA}$  apart from the topmost atoms moving it rigidly by changing the position of Co(II) and the two  $\text{N}_{\text{CN}}$  with respect to the surface  $\text{O}_{2\text{c}}$  and  $\text{Ti}_{5\text{c}}$  atoms and rotating the molecular axis parallel to the surface (more details in ESI). The optimization is carried out by relaxing the molecular geometry and the two top-most layers of the rutile slab. The other three slab layers are kept fixed at bulk coordinates. From these eleven starting positions, only four distinct stable configurations have been obtained. These four structures are displayed in Figure 5 and are named model-a, b, c, and d. The adsorption energy ( $E_{\text{ads}}$ ) is calculated as

$$E_{\text{ads}} = E_{\text{complex}} - (E_{\text{slab}} + E_{\text{mol}}) \quad (2)$$

where  $E_{\text{complex}}$  is the total energy of the complex,  $E_{\text{slab}}$  is the energy of the slab where only two layers are fully optimized, and  $E_{\text{mol}}$  is the energy of the molecule optimized in vacuum. Negative values of  $E_{\text{ads}}$  correspond to exothermic adsorption. For each optimized structure, the amount in dispersion energy is extracted, so that its contribution to the adsorption energy is calculated as

$$E_{\text{ads}}^{\text{disp}} = E_{\text{complex}}^{\text{disp}} - (E_{\text{slab}}^{\text{disp}} + E_{\text{mol}}^{\text{disp}}) \quad (3)$$

The dispersion contribution is always attractive. The distortion energy of CoPy ( $E_{\text{dist}}$ ) is, instead, the increase in molecular energy due to the geometrical changes induced by the interaction with the surface,

$$E_{\text{dist}} = E_{\text{mold}} - E_{\text{mol}} \quad (4)$$

$E_{\text{mold}}$  is the energy of the molecule calculated in vacuum, but with the same coordinates obtained from the complex optimization.

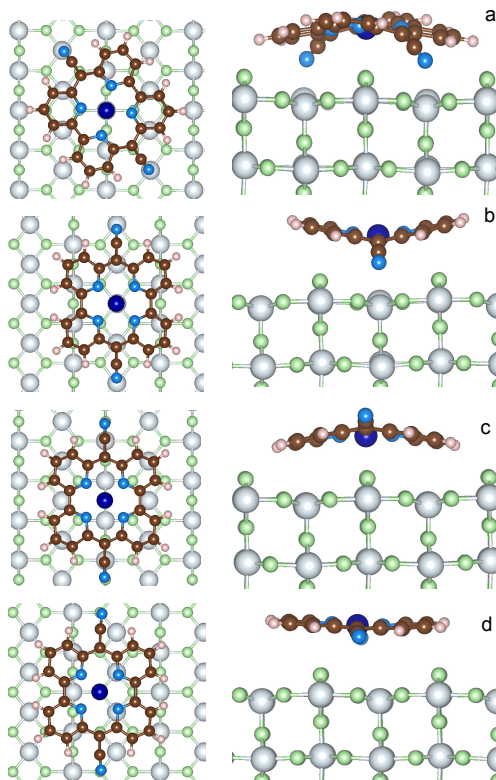


FIG. 5: Four different optimized structures of the CoPy@rutile complex, as obtained from different initial positions of the molecule. The top view (left) and one side view (right) of each of the four models are shown. Color code: see previous figures.

#### IV. RESULTS AND DISCUSSION

The resulting four adsorption configurations of CoPy@rutile are characterized by different energies and structural parameters. In Table V, the above defined  $E_{\text{ads}}$ ,  $E_{\text{ads}}^{\text{disp}}$ ,  $E_{\text{dist}}$  values are reported together with the average height of the molecule on the  $\text{Ti}_{5c}$  layer ( $h_{\text{av}}$ ), the difference in height between the lowest and the highest atoms in the molecule ( $\Delta h$ ), which is a measure of the deviation from planarity, the distance between the two  $\text{N}_{\text{CN}}$  atoms ( $d_{\text{CN}}$ ), and the minimum distance between an atom of the molecule and an atom of the surface ( $d_{\text{min}}$ ).

As a general observation, the interaction to the surface is relatively weak and the major contribution is due to the dispersion term, which varies from 60% to almost 100% of the adsorption energy. The strongest adsorption is obtained for model-a, where the molecule is bent along the  $d_{\text{CN}}$  axes such that both the  $\text{N}_{\text{CN}}$  atoms can sit exactly on top of  $\text{Ti}_{5c}$

TABLE V: Energies and structural parameters characterizing the four distinct adsorption sites reported in Figure 5.

Model	$E_{\text{ads}}$ [eV]	$E_{\text{ads}}^{\text{disp}}$ [eV]	$E_{\text{dist}}$ [eV]	$h_{\text{av}}$ [Å]	$\Delta h$ [Å]	$d_{\text{CN}}$ [Å]	$d_{\text{min}}$ [Å]	pair
a	-4.18	-2.62	0.57	3.67	2.16	10.86	2.13	$\text{N}_{\text{CN}}\text{-Ti}_{5\text{c}}$
b	-3.56	-2.34	0.40	3.89	2.34	11.14	2.22	$\text{N}_{\text{CN}}\text{-Ti}_{5\text{c}}$
c	-3.35	-2.89	0.24	3.52	1.66	11.51	2.25	$\text{Co(II)}\text{-O}_{2\text{c}}$
d	-2.49	-2.42	0.09	3.94	0.95	11.65	2.77	$\text{H-O}_{2\text{c}}$

centers, while Co(II) coordinates two  $\text{O}_{2\text{c}}$ . The interaction is further favored by the upwards displacement of the involved Ti atoms by 0.26 Å, thus reducing the N–Ti distance to only 2.13 Å. CoPy is bent along both axis, even if the curvature is more pronounced along  $d_{\text{CN}}$ , reducing the  $d_{\text{CN}}$  distance by about 1 Å with respect to the gas phase structure. The geometrical changes correspond to a distortion energy of 0.57 eV. Subtracting from the total adsorption energy the distortion energy, we obtain an interaction energy of -4.75 eV, of which -2.62 eV are attributed to dispersion. The remaining -2.13 eV are mainly due to the chemical bonding between  $\text{N}_{\text{CN}}$  and Ti ( $\approx -1$  eV per  $\text{N}_{\text{CN}}$ ), which, as it will be discussed in the following, is responsible for the rehybridization of the molecular homo with the surface states.

In model-b, both  $\text{N}_{\text{CN}}$  and Co(II) are sitting on top of  $\text{Ti}_{5\text{c}}$  centers, and the  $d_{\text{CN}}$  axis is oriented along the [001] lattice direction, i.e. rotated by about 30 degrees with respect to model-a. Also in this case, the closest contact between molecule and surface is the N–Ti interaction, and the involved Ti atoms are displaced upwards by 0.15 Å. However, in this position, some  $\text{O}_{2\text{c}}$  atoms happen to be in proximity of the pyridine rings, which consequently bend outwards. Overall, the distance between molecule and surface ( $h_{\text{av}} = 3.89$  Å) is larger than in model-a, and, even though the molecular distortion energy is smaller, the adsorption interaction is weaker. This can be explained in terms of the repulsive electrostatic interaction between Co(II) and Ti and the reduced dispersion contribution due to the larger average distance.

Like in model-a, in model-c Co coordinates the two closest dangling O. The  $\text{N}_{\text{CN}}$  are on top of the surface oxygen giving rise to a repulsive interaction, which causes the upwards bending along the  $d_{\text{CN}}$  axis. Since only the cyano groups are displaced, the molecule is less

distorted than in the two previous configurations, as also indicated by its  $d_{\text{CN}}$  length and the computed distortion energy. In average, CoPy is closer to the surface and, as a consequence, the dispersion energy term is larger. By subtracting the distortion energy and the dispersion energy from the total adsorption energy, the remaining interaction energy amounts to 0.70 eV.

Finally, in model-d, the most active molecular centers, Co(II) and  $\text{N}_{\text{CN}}$ , are too far from the under-coordinated atoms at the surface. The molecular structure is only slightly modified upon adsorption, since the only attractive interaction is attributed to the dispersion forces. This is a classical example of physisorption, as also confirmed by the almost equal values of  $E_{\text{ads}}$  and  $E_{\text{ads}}^{\text{disp}}$ . Rather weak physisorption has been already reported for the case of a single pyridine ring adsorbed on  $\text{TiO}_2$ <sup>67</sup>.

The standing adsorption of CoPy on rutile(110) surface has also been examined. CoPy is positioned perpendicular to the (110) surface, with one  $\text{N}_{\text{CN}}$  on top of one  $\text{Ti}_{5\text{c}}$ , since between these two species the binding is expected to be strongest. After the optimization of the structure, the distance between  $\text{N}_{\text{CN}}$  and  $\text{Ti}_{5\text{c}}$  is 2.09 Å. The resulting adsorption energy  $E_{\text{ads}}$  is -1.61 eV, i.e. 2.5 eV lower than for the molecule adsorbed flat. The obvious reasons for the weaker binding are that only one direct N- $\text{Ti}_{5\text{c}}$  interaction is available and the significantly smaller contribution of dispersion (-0.65 eV), given the standing geometry.

Pratik et al.<sup>68</sup> modeled several different porphyrin-derived molecules adsorbed both horizontally and vertically on anatase nanoparticles. Their calculations show that while horizontal orientation of porphyrin on anatase has  $E_{\text{ads}}$  of -2.6 eV, porphyrin-4- $\text{NO}_2$  has -9.30 eV, and porphyrin-4- $\text{NH}_2$  has -4.33 eV, vertical attachment of 1- $\text{NMe}_2$ -porphyrin-1-COOH results in  $E_{\text{ads}}$  of -2.80 eV.

In summary, the most effective interactions for the adsorption of CoPy on rutile are those between  $\text{N}_{\text{CN}}$  and the  $\text{Ti}_{5\text{c}}$  surface atoms, followed by the Co(II)- $\text{O}_{2\text{c}}$  coordination. These are maximized in model-a, which turns out to be the most stable adsorption site. Therefore, the following analysis of the electronic properties of the CoPy@rutile is based on this model.

The redistribution of the electronic charge induced by the adsorption is shown in the electron density difference maps. The electron density difference is calculated by subtracting from the total density of the complex  $\rho_{\text{complex}}(\mathbf{r})$  the individual electron densities of CoPy

and the slab, at the same coordinates as in the complex

$$\Delta\rho(\mathbf{r}) = \rho_{\text{complex}}(\mathbf{r}) - (\rho_{\text{slab}}(\mathbf{r}) + \rho_{\text{mol}}(\mathbf{r})). \quad (5)$$

The two isosurfaces of  $\Delta\rho(\mathbf{r})$  in Figure 6 correspond to  $+0.317 \text{ e}/\text{\AA}^3$ , i.e., charge accumulation (top left panel), and  $-0.317 \text{ e}/\text{\AA}^3$  (top right panel), i.e., charge depletion. We notice that the electrons on the pyridine rings are partially pushed away from the surface, to reduce the overlap with dangling orbitals of the  $\text{O}_{2c}$  atoms. On the other hand, electron accumulation is observed between  $\text{N}_{\text{CN}}$  and the closest under-coordinated  $\text{Ti}_{5c}$  atoms, which confirms the presence of a chemical interaction between these species. The rearrangement leads to the polarization of the molecule along the perpendicular axis  $z$ . In panel c of Figure 6 the 2D-integrated density difference calculated as

$$\Delta\rho_{xy}(z) = \int dx \int dy \Delta\rho(\mathbf{r}) \quad (6)$$

is plotted along  $z$ . We observe that a finite dipole moment arises along the  $z$  axis, which, estimated as  $\mu_z = \int \rho_{xy}(z) \cdot z dz$ , amounts to 0.5 D.

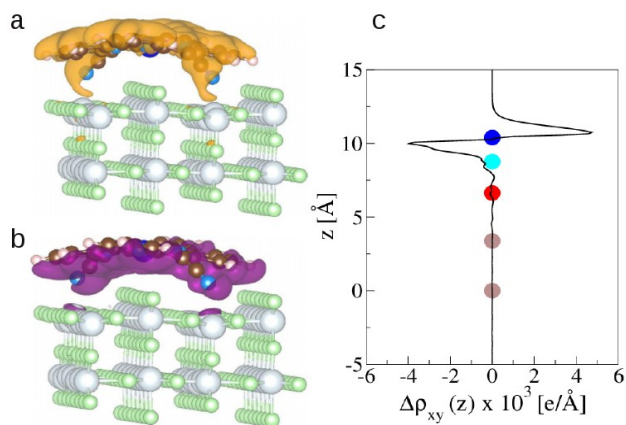


FIG. 6: Electron density difference  $\Delta\rho(\mathbf{r})$ : isosurfaces taken at  $0.317 \text{ e}/\text{\AA}^3$  (a) and  $-0.317 \text{ e}/\text{\AA}^3$  (b). c) 2D integrated density difference  $\Delta\rho_{xy}(z)$  plotted along the slab's perpendicular axis. Red sphere indicates the height of the under-coordinated  $\text{Ti}_{5c}$  atoms, the cyan is  $\text{N}_{\text{CN}}$ , the dark blue  $\text{Co(II)}$ , and the brown spheres are located at the height of two deeper layers.

The total and projected densities of states, TDOS and PDOS, provide further information on the redistribution of the molecular orbitals upon adsorption and on the nature of the interaction. Spin polarization has been used for all calculations; however, not negligible

spin density difference is observed only on Co(II) (see ESI). Therefore, we plot the distinct alpha and beta spin DOS solely for Co(II). We compare the density of states calculated for the CoPy@rutile complex with those calculated for the optimized molecule in the gas phase and for the pristine rutile surface. All PDOS plots related to the complex are aligned with respect to the corresponding VBM and normalized by the number of atoms considered in the projection. In order to facilitate the comparison, the PDOS of the clean rutile (110) slab are rigidly shifted to aligning the bulk states, i.e., the projections on the atoms of the inner layers (third and fourth) to the same states of the CoPy@rutile. These states are not affected by the adsorption and therefore are easily recognizable.

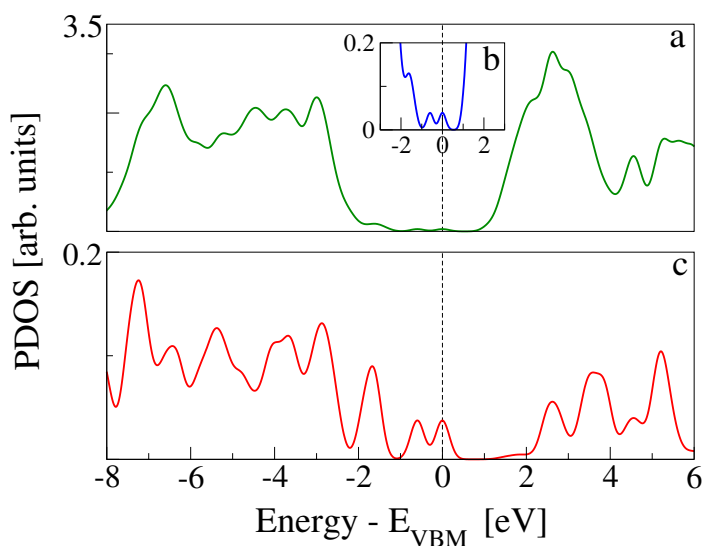


FIG. 7: a) TDOS of CoPy@rutile(110). The inset (b) shows a zoom-in of the energy gap region, which allows to distinguish the molecular states within the rutile energy gap. c) DOS projected on all the atoms of CoPy. Since the number of atoms is much smaller, the normalization factor is different, which allows to better appreciate the fine structure of the molecular states.

In Figure 7, the TDOS of CoPy@rutile (top panel) is compared to the contribution obtained from its projection on the CoPy molecule only (bottom panel). The different normalization factor makes the low intensity features of the molecular states appear with more evidence in the bottom panel. The homo of the complex is clearly a molecular state of CoPy. The lumo, on the other hand, is mainly located on the rutile slab. The calculated energy gap turns out to be 1.06 eV, which is 1.22 eV smaller than the gap of rutile (110).

The lowest unoccupied states with major contributions on CoPy are about 2.5 eV above the VBM.

The effects of CoPy adsorption on the DOS of the slab are evaluated by projecting only on the slab's atoms and comparing to the PDOS computed for the pristine slab. In Figure 8, we distinguish between contributions from surface titanium atoms (b), and surface oxygen atoms (c). The signature of the surface  $\text{Ti}_{5c}$  atoms is the growth in intensity of the left shoulder of the lowest band of unoccupied states, as compared to PDOS of bulk Ti atoms (see Figure 1). The center of this band is at about 1.5 eV. Of the 21  $\text{Ti}_{5c}$  atoms at the surface in our model slab, only two strongly interact with the molecule via the  $\text{N}_{\text{CN}}$  linkers and are responsible for the small difference between the red (CoPy@rutile) and the blue (clean) curves in panel b. The band of the highest occupied states in rutile is mainly constituted of O-2p orbitals. The differences between bulk (see Figure 1) and surface are more evident in this case since the surface oxygen PDOS presents one relatively narrow band at about -3 eV and lower intensity features at lower energies. This pronounced feature is formed by the highest occupied surface states. The effects of CoPy adsorption in the  $\text{O}_{2c}$  PDOS are ascribed to the two surface oxygens interacting with Co(II).

The electronic structure rearrangements occurring upon adsorption have their major effects on the CoPy molecular orbitals. The PDOS on CoPy adsorbed and in the gas phase are compared in Figure 9. All the plots are aligned with the homo at zero eV. The PDOS of CoPy@rutile (red curves) shows a general broadening of the bands. The occupied states on Co(a),  $\text{N}_p$  (b), and C (d) present the same main features as in the gas phase. The lowest unoccupied states are shifted to higher energies by about 0.5 eV. The projected energy gap becomes 0.48 eV larger than the homo-lumo gap in the gas phase, if one considers the lowest unoccupied state with major contributions on the adsorbed molecule, which actually is at 2.5 eV above the homo. The sharp bands characterizing the PDOS on the  $\text{N}_{\text{CN}}$  in the gas phase are most strongly affected by the interaction with the surface. The two localized molecular states at -3.7 eV and -5.5 eV are replaced by a broad distribution due to the re-hybridization with the Ti states. Moreover, the interaction has a clear effect on the charge distribution corresponding to the homo of CoPy. As shown in Figure 10, the orbital extends in the region between molecule and surface, thus strengthening the chemical bonding. This electronic rearrangement explains the bending along  $d_{\text{CN}}$  and the upwards displacement of the Ti atoms.

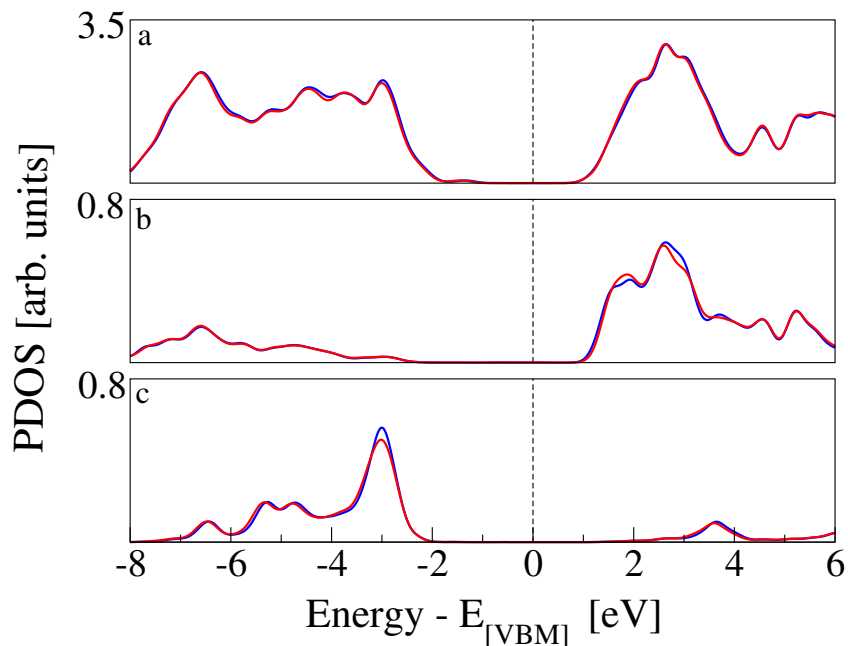


FIG. 8: PDOS related to surface Ti and O atoms of CoPy@rutile(110) (red) and of the clean rutile (110) (blue) are compared. While energy states of CoPy@rutile are aligned with respect to its VBM, alignment in pristine rutile is carried out with respect to highest occupied band of surface O atoms of CoPy@rutile. a) TDOS. b) PDOS on surface under-coordinated Ti centers. c) PDOS on under-coordinated O centers at the surface.

Finally, we separate the contributions to the DOS ascribed to the two  $\text{Ti}_{5c}$  and the two  $\text{O}_{2c}$  atoms more directly involved in the interaction. The resulting PDOS are plotted in Figure 11 and compared with the PDOS obtained from all the  $\text{Ti}_{5c}$  and  $\text{O}_{2c}$  present at the slab surface. While no significant difference is observed among the occupied states, a clear effect of the interaction is present for the lowest unoccupied states localized at  $\text{Ti}_{5c}$ . In particular, we observe the increase in intensity of the first peak and the consequent depletion at higher energies. This result implies the presence of available empty states on the Ti atoms that are also involved in the extension of the molecular homo state. On the other hand, the occupied states localized on the surface O atoms are more than 2 eV lower in energy than the CoPy homo and are not significantly perturbed by the adsorbate.

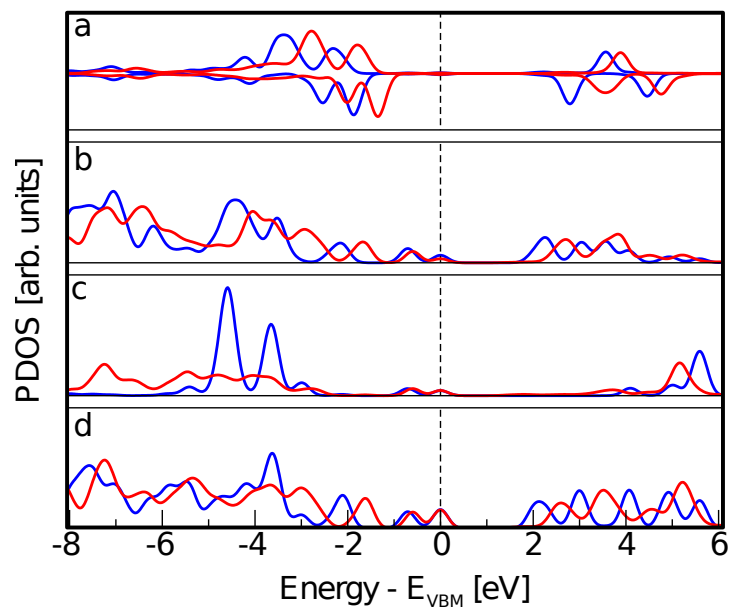


FIG. 9: PDOS on different species of CoPy adsorbed on rutile (red solid line) and optimized in the gas phase (blue solid line). a) PDOS on Co. Positive values are for the alpha spin channel and negative values for the beta spin channel. b) PDOS on the central N atoms binding to the pyridine rings,  $N_p$ . c) PDOS on the external N atoms belonging to the cyano groups,  $N_{CN}$ . d) PDOS on all carbon atoms.

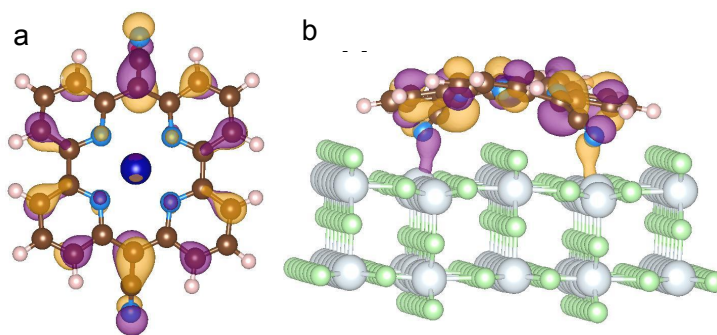


FIG. 10: Representation of the homo of CoPy adsorbed on rutile (110). Top (a) and side (b) view. The displayed isosurfaces are obtained at  $\pm 0.236 \text{ e}/\text{\AA}^3$ .

## V. CONCLUSIONS

We have investigated the adsorption of a porphyrin derived heterocyclic molecule, CoPy, on the rutile (110) surface. This new type of heterocyclic molecules has been experimen-

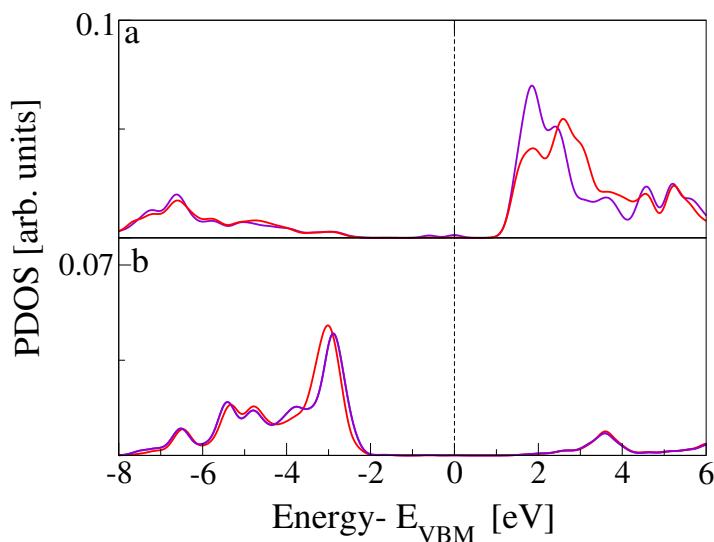


FIG. 11: a) PDOS on  $\text{Ti}_{5c}$  atoms. The red line is the same PDOS shown in panel b of Figure 8, related to the complex. The purple line is related to the only two surface Ti atoms interacting directly with  $\text{N}_{\text{CN}}$ . b) PDOS on  $\text{O}_{2c}$  atoms. Red line is the same PDOS presented in panel c of Figure 8. The purple line is obtained by the projection on the two oxygen atoms coordinating the Co(II) in  $\text{CoPy}@r\text{utile}(110)$ .

tally proved to be an active catalyst for hydrogen evolution reactions. However, there are no extensive studies on its properties and, to our knowledge, this is the first time that the adsorption of one of these has been considered. We observe electronic structure rearrangements occurring upon adsorption, mainly due to the interaction of the cyano groups of CoPy with the five-coordinated Ti atoms of  $\text{rutile}(110)$ . The projected densities of states on the different involved species reveal that the molecular orbitals on the  $\text{N}_{\text{CN}}$  atoms undergo a rehybridization, the homo is located at the molecule, and the lowest unoccupied states of CoPy are shifted to higher energies. Effects of the electronic redistribution are also recognized from the  $\text{Ti}_{5c}$  PDOS and the polarization of the electronic density across the molecular plane. The first band of unoccupied states is mainly on rutile and extends from 1.1 to 2.0 eV, with a maximum at 1.5 eV. The lowest unoccupied states localized on CoPy are instead beyond 2.5 eV, i.e., at higher energy with respect to the lomo of the gas phase molecule. Hence, the adsorption produces a significant reduction of the energy gap with respect to both pristine rutile  $\text{TiO}_2$  and the isolated molecule, which should facilitate absorption of

light in the visible range. This opens the possibility of achieving electron injection from CoPy to rutile, with a consequent efficient electron-hole separation.

On the other hand, but for a rigid shift with respect to the homo, we do not observe strong modifications of the electronic structure at the Co(II) center. From these results we expect that the catalytic properties of CoPy are preserved upon adsorption. We plan to extend the study on this system also considering the co-adsorption of water and hydrogen and possible reaction mechanisms leading to the production of molecular hydrogen. We expect that by functionalizing porphyrin with different linkers and replacing Co with other transition metals, a further tuning of the coupling with the oxide is possible and improved water splitting performance can be achieved.

## VI. ACKNOWLEDGMENTS

We gratefully acknowledge the financial support from the University of Zurich, the University Research Priority Program “Solar Light to Chemical Energy Conversion” (LightChEC), National Centres of Competence in Research–Materials Revolution: Computational Design and Discovery of Novel Materials (NCCR–MARVEL), and computing resources from the Swiss National Supercomputer Centre (CSCS) under the project ID s425.

---

\* yeliz.guerdal@chem.uzh.ch

† sandra.luber@chem.uzh.ch

‡ hutter@chem.uzh.ch

§ marcella.iannuzzi@chem.uzh.ch

<sup>1</sup> W. T. Eckenhoff and R. Eisenberg, *Dalton Transactions* **41**, 13004 (2012).

<sup>2</sup> N. Armaroli and V. Balzani, *Angewandte Chemie International Edition* **46**, 52 (2007).

<sup>3</sup> M. Carmo, D. L. Fritz, J. Mergel, and D. Stolten, *International Journal of Hydrogen Energy* **38**, 4901 (2013).

<sup>4</sup> T. L. LeValley, A. R. Richard, and M. Fan, *International Journal of Hydrogen Energy* **39**, 16983 (2014).

<sup>5</sup> E. Seker, *International Journal of Hydrogen Energy* **33**, 2044 (2008).

- <sup>6</sup> A. T. Ashcroft, A. K. Cheetham, J. S. Foord, M. L. H. Green, C. P. Grey, A. J. Murrell, and P. D. F. Vernon, *Nature* **344**, 319 (1990).
- <sup>7</sup> S. G. Avcioglu, E. Ozgur, I. Eroglu, M. Yucel, and U. Gunduz, *International Journal of Hydrogen Energy* **36**, 11360 (2011).
- <sup>8</sup> M. Grätzel, *Nature* **414**, 338 (2001).
- <sup>9</sup> M. Wang, Y. Na, M. Gorlov, and L. Sun, *Dalton Transactions* , 6458 (2009).
- <sup>10</sup> A. J. Esswein and D. G. Nocera, *Chemical Reviews* **107**, 4022 (2007).
- <sup>11</sup> S. Losse, J. G. Vos, and S. Rau, *Coordination Chemistry Reviews* **254**, 2492 (2010).
- <sup>12</sup> X. Hu, B. S. Brunshwig, and J. C. Peters, *Journal of the American Chemical Society* **129**, 8988 (2007).
- <sup>13</sup> M. Guttentag, A. Rodenberg, R. Kopelent, B. Probst, C. Buchwalder, M. Brandsttter, P. Hamm, and R. Alberto, *European Journal of Inorganic Chemistry* **2012**, 59 (2012).
- <sup>14</sup> H. Imahori and S. Fukuzumi, *Advanced Functional Materials* **14**, 525 (2004).
- <sup>15</sup> L. Si and H. He, *The Journal of Physical Chemistry A* **118**, 3410 (2014).
- <sup>16</sup> B. H. Solis, A. G. Maher, T. Honda, D. C. Powers, D. G. Nocera, and S. Hammes-Schiffer, *American Chemical Society Catalysis* **4**, 4516 (2014).
- <sup>17</sup> S. Soman, *Comments on Inorganic Chemistry* **35**, 82 (2015).
- <sup>18</sup> Z. Han and R. Eisenberg, *Accounts of Chemical Research* **47**, 2537 (2014).
- <sup>19</sup> S. Berardi, S. Drouet, L. Francas, C. Gimbert-Surinach, M. Guttentag, C. Richmond, T. Stoll, and A. Llobet, *Chemical Society Reviews* **43**, 7501 (2014).
- <sup>20</sup> A. Rodenberg, M. Oraziotti, B. Probst, C. Bachmann, R. Alberto, K. K. Baldrige, and P. Hamm, *Inorganic Chemistry* **54**, 646 (2015).
- <sup>21</sup> C. Kutal, *Journal of Chemical Education* **60**, 882 (1983).
- <sup>22</sup> C. G. Garcia, J. F. de Lima, and N. Y. M. Iha, *Coordination Chemistry Reviews* **196**, 219 (2000).
- <sup>23</sup> R. L. Milot, G. F. Moore, R. H. Crabtree, G. W. Brudvig, and C. A. Schmuttenmaer, *The Journal of Physical Chemistry C* **117**, 21662 (2013).
- <sup>24</sup> H. Imahori, S. Kang, H. Hayashi, M. Haruta, H. Kurata, S. Isoda, S. E. Canton, Y. Infahsaeng, A. Kathiravan, T. Pascher, P. Chábera, A. P. Yartsev, and V. Sundström, *The Journal of Physical Chemistry A* **115**, 3679 (2011).
- <sup>25</sup> L.-L. Li and E. W.-G. Diau, *Chemical Society Reviews* **42**, 291 (2013).

- <sup>26</sup> F. Lakadamyali and E. Reisner, *Chemical Communications* **47**, 1695 (2011).
- <sup>27</sup> M. Yin, S. Ma, C. Wu, and Y. Fan, *The Royal Society of Chemistry Advances* **5**, 1852 (2015).
- <sup>28</sup> F. Lakadamyali, A. Reynal, M. Kato, J. R. Durrant, and E. Reisner, *Chemistry – A European Journal* **18**, 15464 (2012).
- <sup>29</sup> D. Achey, S. Ardo, and G. J. Meyer, *Inorganic Chemistry* **51**, 9865 (2012).
- <sup>30</sup> S. Ogawa, R. Narushima, and Y. Arai, *Journal of the American Chemical Society* **106**, 5760 (1984).
- <sup>31</sup> S. Ogawa, T. Uchida, T. Uchiya, T. Hirano, M. Saburi, and Y. Uchidac, *Journal Chemical Society, Perkin Transactions 1* , 1649 (1990).
- <sup>32</sup> C. Pierre, J.-M. Vincent, J.-B. Verlhac, C. Courseille, A. Dautant, and C. Mathoniere, *New Journal of Chemistry* **25**, 522 (2001).
- <sup>33</sup> Z. Zhu, K. Takano, A. Furuham, S. Ogawa, and S. Tsuchiya, *Bulletin of the Chemical Society of Japan* **80**, 686 (2007).
- <sup>34</sup> R. Ibrahim, S. Tsuchiya, and S. Ogawa, *Journal of the American Chemical Society* **122**, 12174 (2000).
- <sup>35</sup> Luttrell Tim, Halpegamage Sandamali, Tao Junguang, Kramer Alan, Sutter Eli, and Batzill Matthias, *Scientific Reports* **4**, 4043 (2014).
- <sup>36</sup> J. Chen, Y.-F. Li, P. Sit, and A. Selloni, *Journal of the American Chemical Society* **135**, 18774 (2013).
- <sup>37</sup> A. G. Thomas and K. L. Syres, *Chemical Society Reviews* **41**, 4207 (2012).
- <sup>38</sup> J. VandeVondele, M. Krack, F. Mohamed, M. Parrinello, T. Chassaing, and J. Hutter, *Computer Physics Communications* **167**, 103 (2005).
- <sup>39</sup> J. VandeVondele and J. Hutter, *The Journal of Chemical Physics* **127**, 114105 (2007).
- <sup>40</sup> S. Goedecker, M. Teter, and J. Hutter, *Physical Review B* **54**, 1703 (1996).
- <sup>41</sup> J. P. Perdew, K. Burke, and M. Ernzerhof, *Physical Review Letters* **77**, 3865 (1996).
- <sup>42</sup> S. Grimme, J. Antony, S. Ehrlich, and H. Krieg, *The Journal of Chemical Physics* **132**, 154104 (2010).
- <sup>43</sup> T. L. Bahers, M. Rérat, and P. Sautet, *The Journal of Physical Chemistry C* **118**, 5997 (2014).
- <sup>44</sup> A. J. Cohen, P. Mori-Snchez, and W. Yang, *Science* **321**, 792 (2008).
- <sup>45</sup> J. Muscat, V. Swamy, and N. M. Harrison, *Physical Review B* **65**, 224112 (2002).

- <sup>46</sup> F. Labat, P. Baranek, and C. Adamo, *Journal of Chemical Theory and Computation* **4**, 341 (2008).
- <sup>47</sup> H. Xiao, J. Tahir-Kheli, and W. A. Goddard, *The Journal of Physical Chemistry Letters* **2**, 212 (2011).
- <sup>48</sup> J. Heyd, G. E. Scuseria, and M. Ernzerhof, *The Journal of Chemical Physics* **118**, 8207 (2003).
- <sup>49</sup> A. V. Krukau, O. A. Vydrov, A. F. Izmaylov, and G. E. Scuseria, *The Journal of Chemical Physics* **125**, 224106 (2006).
- <sup>50</sup> M. Guidon, J. Hutter, and J. VandeVondele, *Journal of Chemical Theory and Computation* **6**, 2348 (2010).
- <sup>51</sup> M. Guidon, J. Hutter, and J. VandeVondele, *Journal of Chemical Theory and Computation* **5**, 3010 (2009).
- <sup>52</sup> M. Guidon, F. Schiffmann, J. Hutter, and J. VandeVondele, *The Journal of Chemical Physics* **128**, 214104 (2008).
- <sup>53</sup> C. J. Howard, T. M. Sabine, and F. Dickson, *Acta Crystallographica Section B* **47**, 462 (1991).
- <sup>54</sup> J. K. Burdett, T. Hughbanks, G. J. Miller, J. W. Richardson, and J. V. Smith, *Journal of the American Chemical Society* **109**, 3639 (1987).
- <sup>55</sup> H. Perron, J. Vandenborre, C. Domain, R. Drot, J. Roques, E. Simoni, J. J. Ehrhardt, and H. Catalette, *Surface Science* **601**, 518 (2007).
- <sup>56</sup> Z. Y. Zhao, *The Journal of Physical Chemistry C* **118**, 4287 (2014).
- <sup>57</sup> H. Perron, C. Domain, J. Roques, R. Drot, E. Simoni, and H. Catalette, *Theoretical Chemistry Accounts* **117**, 565 (2007).
- <sup>58</sup> L. Kavan, M. Grätzel, S. E. Gilbert, C. Klemenz, and H. J. Scheel, *Journal of the American Chemical Society* **118**, 6716 (1996).
- <sup>59</sup> R. Evarestov and Y. Zhukovskii, *Surface Science* **608**, 226 (2013).
- <sup>60</sup> U. Diebold, *Surface Science Reports* **48**, 53 (2003).
- <sup>61</sup> C. Lun Pang, R. Lindsay, and G. Thornton, *Chemical Society Reviews* **37**, 2328 (2008).
- <sup>62</sup> S.-C. Li and U. Diebold, *Journal of the American Chemical Society* **132**, 64 (2010).
- <sup>63</sup> T. R. Esch, I. Gadaczek, and T. Bredow, *Applied Surface Science* **288**, 275 (2014).
- <sup>64</sup> S. Fujiyoshi, T.-A. Ishibashi, and H. Onishi, *The Journal of Physical Chemistry B* **109**, 8557 (2005).
- <sup>65</sup> A. T. Paxton and L. Thiën-Nga, *Physical Review B* **57**, 1579 (1998).

- <sup>66</sup> We also optimized the structure of the second isomer of metal-free pyrphyrin finding that when the two protons reside on the same side the molecule is by 0.23 eV less stable.
- <sup>67</sup> S. Suzuki, Y. Yamaguchi, H. Onishi, T. Sasaki, K. Fukui, and Yasuhiro Iwasawa, *Journal Chemical Society, Faraday Transactions* **94**, 161 (1998).
- <sup>68</sup> S. M. Pratik and A. Datta, *Physical Chemistry Chemical Physics* **15**, 18471 (2013).